

Replace this file with `prentcsmacro.sty` for your meeting,
or with `entcsmacro.sty` for your meeting. Both can be
found at the [ENTCS Macro Home Page](#).

An optimal Inverse Laplace Transform method without positive and negative overshoot – an integral based interpretation¹

Illés Horváth²

MTA-BME Information Systems Research Group, Budapest, Hungary

Zsófia Talyigás³

Technical University of Budapest, Budapest, Hungary

Miklós Telek⁴

Department of Networked Systems and Services, Technical University of Budapest, Budapest, Hungary

Abstract

We propose a numerical inverse Laplace transformation method without overshoot which is derived from matrix exponential (ME) distributions with minimal coefficient of variation. We discuss the properties of the method through an integral based interpretation of numerical inverse Laplace transformation methods belonging to the Abate–Whitt framework. Compared to the previously applied non-overshooting alternative, the “Erlang” method, the error of the proposed method improves from $O(1/n)$ to $O(1/n^2)$ while it maintains the same computational complexity.

Keywords: numerical Inverse Laplace transformation, matrix exponential distribution, overshoot, minimal coefficient of variation.

1 Introduction

The implementation of numerical inverse Laplace transformation in stochastic models where the original function is a probability or probability distribution requires that the inverse transformation procedure preserves the property that the numerical inverse transform is between zero and one. Most numerical inverse transform methods generate positive or negative overshoot which might result in numerical

¹ This work is partially supported by the OTKA K123914 project.

² Email:horvath.illes.antal@gmail.com

³ Email:talyigas.zsofi@gmail.com

⁴ Email:telek@hit.bme.hu

inverse transform values below zero or above one, which is an unacceptable qualitative error in stochastic modelling. That is why we focus on the numerical inverse transformation procedures without overshoot in this work.

There are plenty of numerical inverse Laplace transformation methods published in the literature, whose survey is out of the scope of the current work. For a relatively recent initial pointer we refer to [13] and the references therein, however the application field of our focus is significantly different. While a large part of the literature, including mentioned one, lists plenty of methods, a clear and systematic classification of these methods is not easy to find. One exception that significantly helped the intuitive understanding of the authors is by Abate and Whitt in [8], which we refer to as Abate–Whitt framework. Indeed, this framework implicitly defines function families in which various optimizations can be performed in order to obtain optimal inverse Laplace transformation methods. We propose a procedure which is based on the most general function family of the Abate–Whitt framework (referred to as Class III, later on) where we adopt a restriction coming from the non-overshooting requirement. It turns out that the obtained functional optimization problem is known in probability theory as the problem of Matrix exponential distribution with minimal coefficient of variation. As a result, in the current work we apply available extremal results for Matrix exponential distribution for optimal numerical inverse Laplace transformation without overshooting in the Abate–Whitt framework.

The rest of the paper is organized as follows. Section 2 provides general introduction to inverse Laplace transformation and presents the Abate–Whitt framework together with some of its methods. Section 3 is devoted to the integral based interpretation of the framework. The proposed matrix exponential distribution based procedure is described in Section 4 and its performance is compared with other methods from the Abate–Whitt framework in Section 5. The paper is concluded in Section 6.

2 Inverse Laplace transformation and the Abate–Whitt framework

For a real or complex valued function $h(t)$ the Laplace transform is defined as

$$h^*(s) = \int_{t=0}^{\infty} e^{-st} h(t) dt. \quad (1)$$

and the inverse transform problem is to find an approximate value of h at point T (i.e., $h(T)$) based on $h^*(s)$.

Remark 2.1 We assume that $\int_{t=0}^{\infty} e^{-st} h(t) dt$ is finite for $\text{Re}(s) > 0$ thus $h^*(s)$ is well-defined by (1) for $\text{Re}(s) > 0$. For $\text{Re}(s) \leq 0$, $h^*(s)$ is the analytic continuation of $h^*(s)$ for $\text{Re}(s) > 0$.

Remark 2.2 We assume that $h(t)$ is real in this work. As a result, $h^*(\bar{s}) = \bar{h}^*(s)$ and $h^*(\bar{s}) + h^*(s) = 2\text{Re}(h^*(s))$.

Our main interest is inverse Laplace transformation without overshooting. Due

to this reason we restrict our attention to the Abate–Whitt framework which we summarize below.

2.1 The Abate–Whitt framework

The idea is to approximate h by a finite linear combination of the transform values, via

$$h(T) \approx h_n(T) := \sum_{k=1}^n \frac{\eta_k}{T} h^* \left(\frac{\beta_k}{T} \right), \quad T > 0, \quad (2)$$

where the nodes β_k and weights η_k are complex numbers, which depend on n , but not on the transform h^* or the time argument t . This framework was introduced and investigated by Abate and Whitt in [8]. When $h(t)$ in (1) is real valued it can be approximated by the real part of the weighted transform values:

$$\operatorname{Re}(h(T)) \approx \operatorname{Re}(h_n(T)) = \sum_{k=1}^n \operatorname{Re} \left(\frac{\eta_k}{T} h^* \left(\frac{\beta_k}{T} \right) \right).$$

In the special case when there is a complex conjugate pair among the nodes and weights (that is, $\eta_i = \bar{\eta}_j$ and $\beta_i = \bar{\beta}_j$) then

$$\frac{\eta_i}{T} h^* \left(\frac{\beta_i}{T} \right) + \frac{\eta_j}{T} h^* \left(\frac{\beta_j}{T} \right) = 2 \operatorname{Re} \left[\frac{\eta_i}{T} h^* \left(\frac{\beta_i}{T} \right) \right].$$

We consider three classic algorithms of the Abate–Whitt framework: the Gaver–Stehfest method, the Euler method and the Talbot method. All three were already investigated by Abate and Whitt [8]. We now give a different approach and also compare them with the matrix exponential method we propose.

The Gaver–Stehfest algorithm is based on the sequence of Gaver approximants, derived by Gaver [5]. Since the convergence of the Gaver approximants was only logarithmic, it needed acceleration. A linear acceleration method was proposed by Stehfest [10], using the Salzer acceleration scheme. As it is observed in [8], the accelerated version fits in framework (2), so we can investigate it in this class.

Euler’s method and its derivation can be found e.g. in [1]. In [8] it is rewritten in a form that fits the structure of (2).

Talbot’s algorithm was first introduced by A. Talbot in 1979 in [11]. The version of the form of (2) is derived in [8] based on an earlier work of Abate and Valko [12].

The three methods in question all approximate $h(t)$ by $h_n(t)$, where $h_n(t)$ has structure (2) with weights η_k and nodes β_k , $k = 1, 2, \dots, n$. The weights and nodes for the considered algorithms are given below.

Gaver–Stehfest method (for even n)

$$\beta_k = k \ln(2), \quad 1 \leq k \leq n$$

$$\eta_k = \ln(2) (-1)^{n/2+k} \sum_{j=\lfloor (k+1)/2 \rfloor}^{\min(k, n/2)} \frac{j^{n/2+1}}{(n/2)!} \binom{n/2}{j} \binom{2j}{j} \binom{j}{k-j}, \quad 1 \leq k \leq n$$

where $\lfloor x \rfloor$ is the greatest integer less than or equal to x .

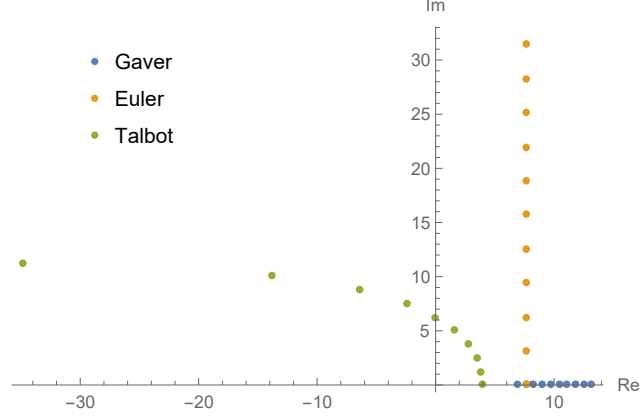


Figure 1. Location of β_k nodes on the complex plane for Gaver ($n = 10$), Euler ($n = 11$), Talbot ($n = 10$) methods

Euler method (for odd n)

$$\beta_k = \frac{(n-1)\ln(10)}{6} + \pi i(k-1), \quad 1 \leq k \leq n$$

$$\eta_k = 10^{(n-1)/6}(-1)^k \xi_k, \quad 1 \leq k \leq n$$

where

$$\xi_1 = \frac{1}{2}$$

$$\xi_k = 1, \quad 2 \leq k \leq (n+1)/2$$

$$\xi_n = \frac{1}{2^{(n-1)/2}}$$

$$\xi_{n-k} = \xi_{n-k+1} 2^{-(n-1)/2} \binom{(n-1)/2}{k} \text{ for } 1 \leq k < (n-1)/2.$$

Talbot method

$$\beta_1 = \frac{2n}{5}$$

$$\beta_k = \frac{2(k-1)\pi}{5} \left(\cot\left(\frac{(k-1)\pi}{n}\right) + i \right), \quad 2 \leq k \leq n$$

$$\eta_1 = \frac{1}{5} e^{\beta_1}$$

$$\eta_k = \frac{2}{5} \left[1 + i \frac{(k-1)\pi}{n} \left(1 + \left[\cot\left(\frac{(k-1)\pi}{n}\right) \right]^2 \right) - i \cot\left(\frac{(k-1)\pi}{n}\right) \right] e^{\beta_k}, \quad 2 \leq k \leq n.$$

Figure 1 depicts the location of the β_k nodes of the three methods. The Gaver–Stehfest method operates with real β_k values which is beneficial when complex arithmetic is not supported, while the Euler and Talbot methods apply complex β_k values as well. Both assume nodes with positive imaginary parts. The Talbot method applies β_k values with negative real part as well, which is commonly outside of the convergence region of (1), but the analytic continuation of $h^*(s)$ may exist.

Remark 2.3 The set of real valued functions $\sum_k \eta_k e^{-\beta_k t}$ with potentially complex valued coefficients has the following real representations.

Class I If both η_k and β_k are real then $\sum_k \eta_k e^{-\beta_k t}$ is a real representation.

Class II If η_k is real and β_k is complex then

$$\operatorname{Re} \left(\sum_k \eta_k e^{-\beta_k t} \right) = \sum_k \eta_k e^{-b_k t} \cos(\omega_k t)$$

is its real representation, where $\beta_k = b_k + i\omega_k$.

Class III If both η_k and β_k are complex then

$$\operatorname{Re} \left(\sum_k \eta_k e^{-\beta_k t} \right) = \sum_k a_k e^{-b_k t} \cos(\omega_k t + \phi_k)$$

is its real representation, with $\operatorname{Re}(\eta_k e^{-\beta_k t}) = a_k e^{-b_k t} \cos(\omega_k t + \phi_k)$ where $\beta_k = b_k + i\omega_k$ and a_k, ϕ_k are real and obtained from the real and imaginary parts of η_k [6].

The Gaver–Stehfest method falls into Class I, the Euler method falls into Class II, the Talbot method falls into Class III. The matrix exponential method (described in detail in Section 4.4) falls into Class III.

3 Integral interpretation of the Abate–Whitt framework

For $\operatorname{Re}(\beta_k) > 0, \forall k$, we can reformulate the inverse Laplace transformation methods of the Abate–Whitt framework as

$$h_n(T) = \frac{1}{T} \sum_{k=1}^n \eta_k h^* \left(\frac{\beta_k}{T} \right) = \frac{1}{T} \sum_{k=1}^n \eta_k \int_0^\infty e^{-\frac{\beta_k}{T} t} h(t) dt = \int_0^\infty h(t) f_T^n(t) dt, \quad (3)$$

where the numerical approximation of the Laplace inverse at point T is obtained as the integral of the original function, $h(t)$, with

$$f_T^n(t) = \frac{1}{T} \sum_{k=1}^n \eta_k e^{-\frac{\beta_k}{T} t}. \quad (4)$$

If $f_T^n(t)$ was the Dirac impulse function at point T then the Laplace inversion would be perfect, but depending on the order of the approximation (n), the applied inverse transformation method (weights η_k , nodes β_k) and the time point (T), function $f_T^n(t)$ only approximates the Dirac impulse function with a given accuracy.

The shape of $f_T^n(t)$ is similar to the shape of

$$f_1^n(t) = \sum_{k=1}^n \eta_k e^{-\beta_k t} \quad (5)$$

because, according to (4),

$$f_T^n(t) = \frac{1}{T} f_1^n\left(\frac{t}{T}\right). \quad (6)$$

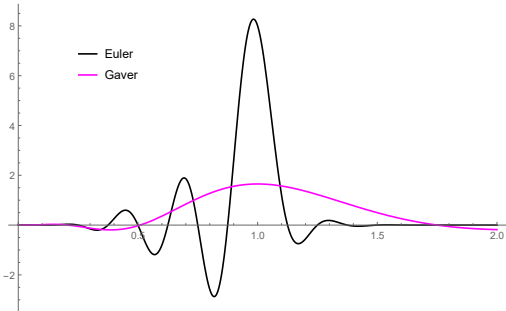


Figure 2. $f_T^n(t)$ for the Gaver–Stehfest ($n = 10$) and the Euler ($n = 11$) methods for $T = 1$

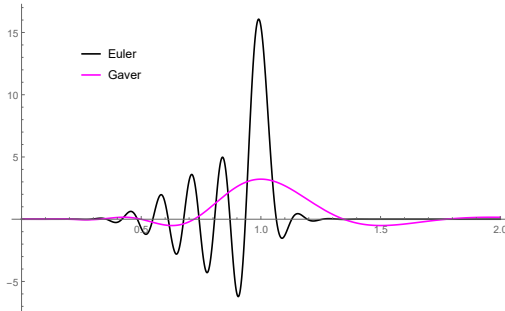


Figure 3. $f_T^n(t)$ for the Gaver–Stehfest ($n = 22$) and the Euler ($n = 23$) methods for $T = 1$

The $\text{Re}(\beta_k) > 0, \forall k$ property holds for the Euler and the Gaver–Stehfest methods, but not for the Talbot method (c.f. Fig. 1). Figure 2 and 3 depicts the approximate Dirac impulse functions for $n = 11$ and $n = 23$ for the Euler and $n = 10$ and $n = 22$ for the Gaver–Stehfest methods at $T = 1$. In accordance with expectations, the functions get visually “narrower” (more concentrated) for higher orders in both cases. For a more quantitative comparison we collected some properties of the functions $f_T^n(t)$ in Table 1.

We introduce a measure of concentration from probability theory, the coefficient of variation (cv). For a random variable X with probability density function f , $\text{cv}(X)$ is defined as

$$\text{cv}(X) = \frac{\text{var}(X)}{(\mathbb{E}(X))^2} = \frac{m_2}{m_1^2} - 1, \quad \text{where } m_i = \int_t t^i f(t) dt.$$

Our goal is to measure how concentrated f_T^n is. Note that f_T^n is not necessarily a proper normalized pdf, since we allow its integral to be different from 1 and f_T^n may take negative values. However, it is possible to introduce cv for f_T^n , and it will be informative later on. The coefficient of variation for f_T^n is defined as

$$\text{cv} = \frac{m_0 m_2}{m_1^2} - 1, \quad \text{with } m_i = \int_t t^i |f_T^n(t)| dt.$$

(The use of m_0 is necessary if f_T^n is not normalized.)

We introduce some further measures that help quantify the concentration of f_T^n : *peak* denotes the maximal value of f_T^n , while *min* and *max* denote the first point and the last point where $f_T^n(t) = 0.01 \text{peak}$ (where 0.01 is arbitrarily chosen). The main impulse of the Euler method is much higher and narrower than the one for the Gaver–Stehfest method for both orders as indicated by the *peak* values and the distance of the zeros ($f_T^n(t) = 0$) closest to $t = 1$. This trend is also visible on the *min* and *max* values (*min* increases/*max* decreases with n , and Euler is narrower than Gaver–Stehfest), except the *min* value of the Euler method. The particular value, $\text{min} = 0.376047$, is due to a local maximum only a little larger than 0.01max (if that peak was less than 0.01max then *min* would be around 0.474721, see Fig.

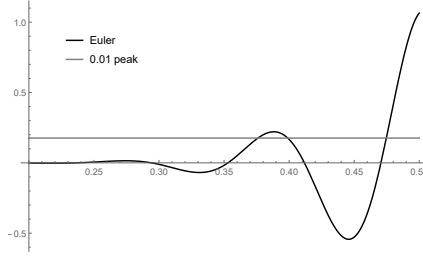


Figure 4. Local peak of $f_T^n(t)$ at around $0.01peak$ (horizontal line) with Euler $n = 11$, $T = 1$

4), but the increase of min for the Euler method is significantly slower than the one for the Gaver–Stehfest method.

For a properly scaled numerical inverse Laplace transformation method, $f_T^n(t)$ should preserve the integral property of the Dirac impulse, that is,

$$\int_t f_T^n(t) dt = 1,$$

and the weight and node parameters of the Gaver–Stehfest and the Euler methods are indeed such that the unit integral is ensured for all orders. Having the unit integral property, a larger m_0 indicates that the function $f_T^n(t)$ is “waving” between positive and negative values more. m_0 is higher and more rapidly increasing with the order for the Euler method. This fact together with the slowly increasing min value indicate that the $f_T^n(t)$ function of the Euler method is sharply alternating mainly before the main impulse and this strong waving behaviour gets more significant with increasing order (see Figures 2 and 3 again).

A cumulative effect of the properties discussed above is reflected in the cv values. For $n = 11$, the Euler method provides much lower cv due to the relatively narrow non-vanishing curve (from min to max), but with increasing order the min value of the Euler method does not increase as fast as for the Gaver–Stehfest method and the waving of the Euler curve from min to the main impulse gets more and more dominant. As a consequence of these two effects, the cv value of the Euler method decreases much slower than the one of the Gaver–Stehfest method.

n	m_0	cv	$peak$	min	max
Gaver					
10	1.32819	0.261505	1.65108	0.0969432	3.94368
22	1.46379	0.0950682	3.53038	0.359999	2.10102
Euler					
11	1.79425	0.0395198	8.26811	0.383763	1.34461
23	2.47539	0.0299859	17.6272	0.376047	1.16585

Table 1
Properties of $f_T^n(t)$ with the Gaver–Stehfest ($n = 10, 22$) and the Euler ($n = 11, 23$) methods at $T = 1$

As we have seen, for a given order the $f_T^n(t)$ function by the Euler method is much narrower than the one by the Gaver–Stehfest method. This difference comes also from the fact that the β_k values of the Gaver–Stehfest method are real, while they are complex in case of the Euler method, while the η_k values are real in both cases (c.f., Remark 2.3). As a result $f_T^n(t) = \sum_{k=1}^n \frac{a_k}{T} e^{-\frac{b_k}{T} t}$ (with real a_k, b_k) for the Gaver–Stehfest method and $f_T^n(t) = \sum_{k=1}^n \frac{a_k}{T} e^{-\frac{b_k}{T} t} \sin(\frac{\omega_k}{T} t)$ (with real a_k, b_k, ω_k) for

the Euler method, that is, the Euler method approximates the Dirac impulse using a larger set of exponential functions.

Up to this point we investigated the main properties of the $f_T^n(t)$ functions. Below we study the effect of these properties on the inverse transform computed by the Gaver–Stehfest and the Euler methods. The Gaver–Stehfest and the Euler Laplace inversion of the unit step function at 1 (denoted by $h(t)$ and with Laplace transform) $h^*(s) = \frac{e^{-s}}{s}$, are depicted in Figure 5 for $n = 10/11$ and in Figure 6 for $n = 22/23$.

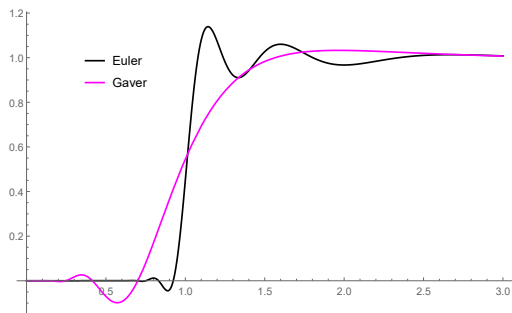


Figure 5. Inverse Laplace transform of the unit step function with Gaver–Stehfest ($n = 10$) and Euler ($n = 11$) methods

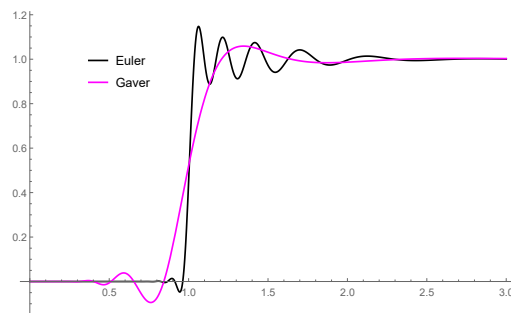


Figure 6. Inverse Laplace transform of the unit step function with Gaver–Stehfest ($n = 22$) and Euler ($n = 23$) methods

The increase of the inverse Laplace curve at around $t = 1$ is the steepest for the Euler method with $n = 23$ and slowest for the Gaver–Stehfest method with $n = 10$. This steepness is associated with the width of the main peak in the $f_T^n(t)$ function (see also the related discussion on the waves based on (7)).

In general, a wider $f_T^n(t)$ function makes the $h(t)f_T^n(t)$ product non-vanishing for t values far from T and as a consequence the $\int_t h(t)f_T^n(t)dt$ integral is affected by $h(t)$ for values of t far from T as well. The error caused by the width of $f_T^n(t)$ is less significant if $h(t)$ is almost constant around T , but it gets to be very significant when $h(t)$ sharply changes around T in the range of the width of $f_T^n(t)$ (like in the case of the unit step function).

As a counterpart of the sharp increase the Euler inverse Laplace curve has a strongly waving behaviour mainly after the jump, while the Gaver–Stehfest curve settles more quickly. To better relate $f_T^n(t)$ and $h_n(T)$ in this special case (where $h(t) = 1$ for $t > 1$ and zero otherwise) we write

$$h_n(T) = \int_0^\infty h(t)f_T^n(t)dt = \int_1^\infty f_T^n(t)dt \quad (7)$$

and depict $f_{1.14}^{11}(t)$ of the Euler method in Figure 7, because the first peak of the Euler $n = 11$ inverse Laplace curve on Figure 5 after the step is at $t = 1.14$. The integral of $f_{1.14}^{11}(t)$ from 1 to infinity is maximal, because it starts right at the end of the largest negative wave. Following the same reasoning one can see that the waves of the Euler inverse Laplace curve after the step are related with the waves of the $f_T^n(t)$ function before the main impulse and similarly the waves of the Euler inverse Laplace curve before the step are related with the waves of the $f_T^n(t)$ function after the main impulse. Since the $f_T^n(t)$ function of the Euler method is heavily alternating before the main impulse the Euler inverse transform curve of

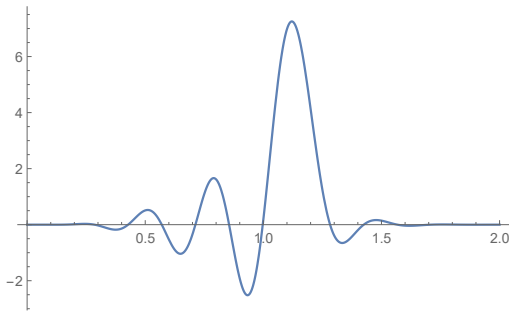


Figure 7. $f_{1.14}^{11}(t)$ with the Euler method. Its integral from 1 to ∞ is maximal.

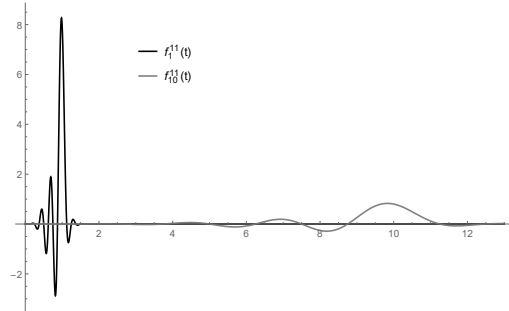


Figure 8. Scaling at $T = 10$: $f_1^{11}(t)$ and $f_{10}^{11}(t)$ with the Euler method

any jump have small waves before the jump and larger waves after the jump (as it is seen e.g. in Fig. 5 and 6).

The unit step function at 1 is a valid probability function in the sense that $0 \leq h(t) \leq 1, \forall t > 0$. As it is discussed in details the alternating nature of $f_T^n(t)$ generates waves in the transform domain curve, which goes below zero before the step and above one after the step. That is, both, the Euler and the Gaver–Stehfest method overshoots at a jump of $h(t)$ and provide numerical inverse outside the $[0, 1]$ interval. To obtain a numerical inverse of the unit step function inside the $[0, 1]$ interval, $f_T^n(t)$ should be nonnegative, which is violated by both the Euler and the Gaver–Stehfest methods and which is the subject of the next sections.

4 Matrix exponential distributions

4.1 Probability background

Probability density functions (pdf) similar to the form (5) have been examined for a long time [2]. The class of matrix exponential distributions of order N , denoted $\text{ME}(N)$, contains all distributions X with pdf of the form

$$f_X(t) = -\alpha \mathbf{A} e^{\mathbf{A}t} \mathbf{1}, \quad t \geq 0, \quad (8)$$

where α is a row vector of length N , \mathbf{A} is a matrix of size $N \times N$ and $\mathbf{1}$ is a column vector of ones of size N .

Rewriting (8) based on the Jordan decomposition of \mathbf{A} , we obtain the following general form of ME functions:

$$f_X(t) = \sum_{i=1}^k \sum_{j=0}^{\ell_i-1} c_{i,j} t^j e^{\lambda_i t}, \quad (9)$$

where $\lambda_1, \dots, \lambda_k$ are eigenvalues of \mathbf{A} , and λ_i has multiplicity ℓ_i . The form (9) is not quite consistent with (5) since (9) may contain polynomial factors as well; nevertheless, if $f_1^n(t)$ (as defined in (5)) is nonnegative, then $f_1^n(t) \in \text{ME}(N)$.

For a given $f_X(t)$, α and \mathbf{A} are not unique; if (8) holds, we say that X is matrix exponentially distributed with representation (α, \mathbf{A}) , or $X \sim \text{ME}(\alpha, \mathbf{A})$ for short. $f_X(t)$ is normalized (that is, $\int_0^\infty f_X(t) dt = 1$) iff $\alpha \mathbf{1} = 1$. This is usually assumed.

The nonnegativity of $f_X(t)$ does not follow from either (8) or (9), and needs to be checked separately.

A special subclass of $\text{ME}(N)$ is the phase-type distributions $\text{PH}(n)$: if, in addition to (8), we also assume that

- $\alpha_i \geq 0$,
- $A_{i,j} \geq 0$ for $i \neq j$, $A_{j,j} < 0$,
- $\mathbf{A}\mathbf{1} \leq 0$

then we say X is phase type (PH) distributed. Phase type distributions have a nice stochastic interpretation: X is the absorption time of an absorbing continuous time Markov chain with a finite state space of size N with infinitesimal generator \mathbf{A} and initial distribution α . As a consequence, nonnegativity of $f_X(t)$ follows from the additional assumptions.

Evidently, $\text{PH}(N) \subseteq \text{ME}(N)$; however, the difference is not well understood in general.

4.2 Concentrated PH and ME distributions

For the class $\text{PH}(N)$, the minimal cv is known. Aldous and Shepp [4] have proven the following theorem:

Theorem 4.1

$$\min_{X \in \text{PH}(N)} \text{cv}(X) = \frac{1}{N}, \quad (10)$$

and the minimum is obtained for the Erlang distribution with parameters (N, λ) where $\lambda > 0$ is arbitrary.

For the class $\text{ME}(N)$, the minimal cv has been calculated in [6], with the following conjecture based on numerical optimization for odd values of N up to $N = 47$:

$$\min_{X \in \text{ME}(N)} \text{cv}(X) \sim \frac{2}{N^2}, \quad (11)$$

and the optimal matrix exponential distribution was of the following form (assuming odd N):

$$f_{\text{ME}}(t) = c e^{-\lambda t} \prod_{i=0}^{(N-1)/2} \cos^2(\omega t - \phi_i) \quad (12)$$

with the real values of c, λ, ω and $\phi_1, \dots, \phi_{(N-1)/2}$ obtained from numerical optimization.

4.3 Erlang distribution-based inverse Laplace transformation

In this paper, we would like to emphasize the benefit of using ME-based inverse Laplace transformation compared to the commonly applied non-overshooting in-

verse Laplace transformation method, based on Erlang distribution [3,9]. The Erlang distribution has pdf

$$f_{\text{Erlang}}(t) = \frac{\lambda^N}{(N-1)!} t^{N-1} e^{-\lambda t},$$

which is not consistent with (5) due to the polynomial factor t^{N-1} .

For the inverse Laplace transformation, the polynomial factor t^{N-1} corresponds to

$$\frac{d^{N-1}}{ds^{N-1}} h^*(s),$$

which technically does not fit in Class III. While calculating or approximating the $(N-1)$ th derivative may be infeasible in general, efficient methods are available for some applications. For example, Asmussen, Avram and Usabel [3] use it to approximate the probability of ruin in a fluid model before a fixed time T .

4.4 ME distribution-based inverse Laplace transformation

Our main focus is the application of the concentrated ME distribution described in (12) for inverse Laplace transformation. (12) can be rewritten in a form consistent with either (8) or (5):

$$f_{\text{ME}}(t) = c e^{-\lambda t} \prod_{i=0}^{(N-1)/2} \cos^2(\omega t - \phi_i) = \sum_{i=1}^N \eta_i e^{-\beta_i t} = \eta_1 e^{-\beta_1 t} + 2 \sum_{i=2}^n \text{Re} \left(\eta_i e^{-\beta_i t} \right) \quad (13)$$

where $n = (N+1)/2$, η_1, β_1 are real, and the values β_2, \dots, β_n have positive imaginary parts. For details, see the Appendix of [6]. Using the function (13) in (4) and (3) is what we call the ME based inverse Laplace transformation method.

A full list of the values of $\eta_1 \dots \eta_n, \beta_1, \dots, \beta_n$ for each n up to $n = 24$ is available online at [7]. As an example, we include the values for $n = 4$ ($N = 7$). The imaginary parts of β_1, \dots, β_n form an arithmetic sequence due to the special form of (12) (see the Appendix in [6]).

i	1	2	3	4
η_i	38.5032	$-18.9855 - 23.2984i$	$-2.70326 + 13.374i$	$2.47829 - 1.37694i$
β_i	-3.93763	$-3.93763 + 3.48448i$	$-3.93763 + 6.96896i$	$-3.93763 + 10.4534i$

5 Numerical comparison with the ME based method

In this section we compare the proposed matrix exponential method (ME method) with the three known algorithms from the Abate–Whitt framework (Euler, Talbot, Gaver–Stehfest) via numerical examples. It is investigated how well the methods approximate h when h^* is given. We compare the different algorithms for the same order n , where n refers to the number nodes at which h^* is evaluated. Note that the Euler method is only applicable for odd order and the Gaver–Stehfest method

is only applicable for even order. Thus for each n tested, either the order of the Euler method or the order of the Gaver–Stehfest method is shifted by 1 compared to the others.

Table 2 contains the Laplace transform pairs of the list of test functions, h and h^* .

$h(t)$	e^{-t}	$\sin t$	$\mathbb{1}(t > 1)$	$\mathbb{1}(t > 1)e^{1-t}$	$[t]$	square wave function
$h^*(s)$	$\frac{1}{1+s}$	$\frac{1}{s^2+1}$	$\frac{1}{s}e^{-s/2}$	$\frac{e^{-s}}{1+s}$	$\frac{1}{s} \frac{1}{e^s-1}$	$\frac{1}{s} \frac{1}{e^s+1}$

Table 2
Set of test functions

Figures 9 and 10 depict the approximations for $h(t) = e^{-t}$ with the various methods for order $n = 3$ ($n = 4$ for Gaver–Stehfest) and $n = 5$ ($n = 6$ for Gaver–Stehfest) respectively. The approximations are relatively accurate already for order $n = 5$ for all methods.

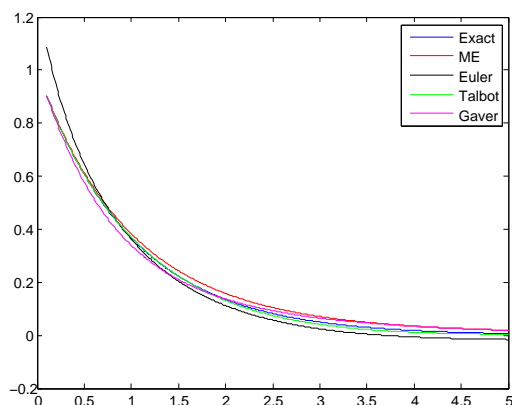


Figure 9. $h(t) = e^{-t}$ for order $n = 3$ (Gaver: $n = 4$)

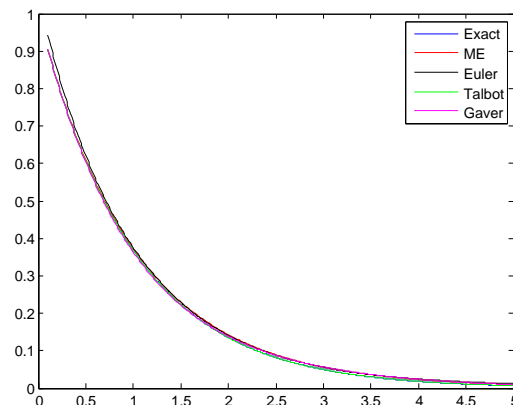


Figure 10. $h(t) = e^{-t}$ for $n = 5$ (Gaver: $n = 6$)

Figures 11 and 12 depict the approximations for $h(t) = \sin(t)$ with the various methods for order $n = 13$ ($n = 14$ for Gaver–Stehfest) and $n = 24$ ($n = 25$ for Euler) respectively. Note that the approximation gets worse for larger values of T . This is inherent to all Abate–Whitt class methods since in (3), the approximant for the Dirac impulse function $f_T^n(t)$ is scaled from $f_1^n(t)$ according to (6) and thus $f_T^n(t)$ is less concentrated for larger values of T . Figure 8 demonstrates this effect for $f_1^{11}(t)$ and $f_{10}^{11}(t)$ with the Euler method. Intuitively, when the main impulse of $f_T^n(t)$ is wider than a period of the sinus wave, then the integral in (3) averages out the waves.

That said, the rate at which the approximation becomes worse as T increases is different for different methods. The Talbot and Gaver–Stehfest methods provide relatively poor approximations with the functions near constant 0 after only two periods for $n = 13$ and three periods for $n = 24$.

The Euler method provides relatively accurate approximation for 4 periods for $n = 14$ and 7 periods for $n = 25$; the overshooting is visible as the Euler-method also provides values larger than 1 and values smaller than -1 (outside the range of the original function $\sin(t)$). The period is also distorted for larger values of t , shifting the local extrema (due to the strong asymmetry of $f_T^n(t)$ with the Euler method).

Also, the “amplitude” of the function provided by the Euler-method decays rather abruptly.

The matrix exponential method retains the periodic nature of $\sin(t)$, it does not overshoot, retains the period length as well, but the amplitude decays gradually. Overall, the Euler method provides the best approximation for $\sin(t)$, but with some overshooting.

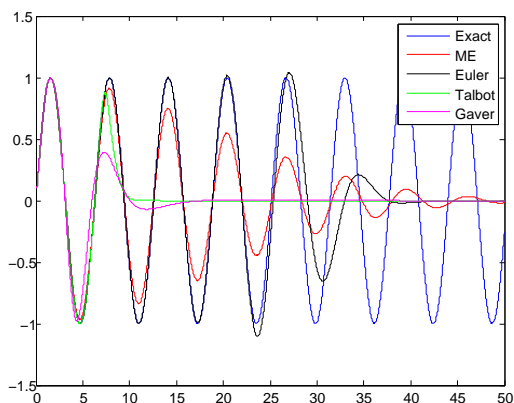


Figure 11. $h(t) = \sin(t)$ for $n = 13$ (Gaver: $n = 14$)

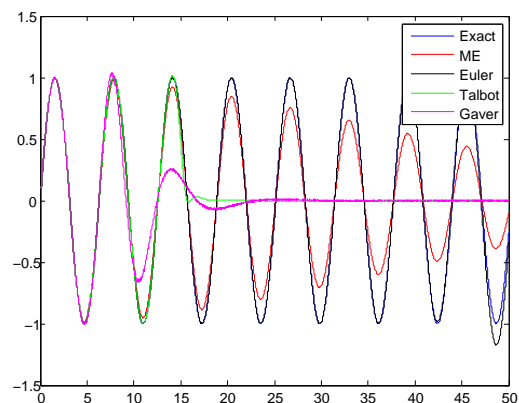


Figure 12. $h(t) = \sin(t)$ for $n = 24$ (Gaver: $n = 25$)

Figures 13 and 14 depict the approximations for the step function $h(t) = \mathbf{1}(t > 1)$ for order $n = 13$ ($n = 14$ for Gaver–Stehfest) and $n = 24$ ($n = 25$ for Euler) respectively. The Talbot method was omitted since it would sample values of $h^*(s)$ outside the domain of convergence of the integral. The other methods provide a reasonable approximation; note that again, the Gaver–Stehfest and the Euler methods overshoot. Note also that the “size” of the overshooting does not decrease with the order vertically, only horizontally. The matrix exponential method does not overshoot, and provides the best approximation overall.

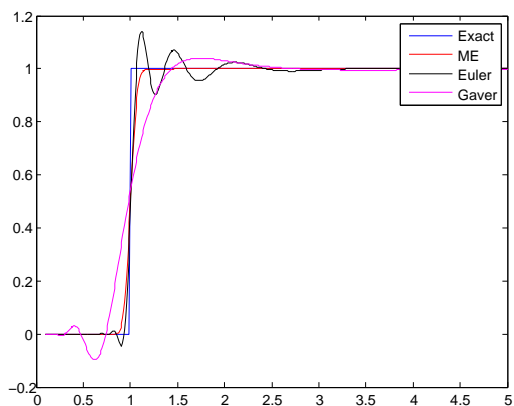


Figure 13. $h(t) = \mathbf{1}(t > 1)$ for $n = 13$ (Gaver: $n = 14$)

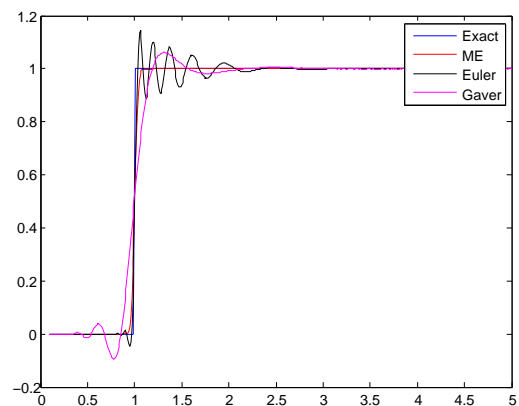
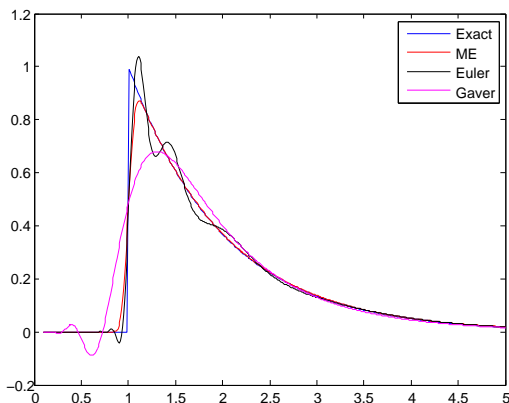
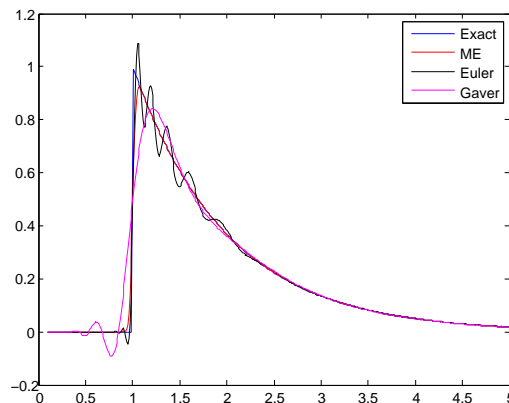
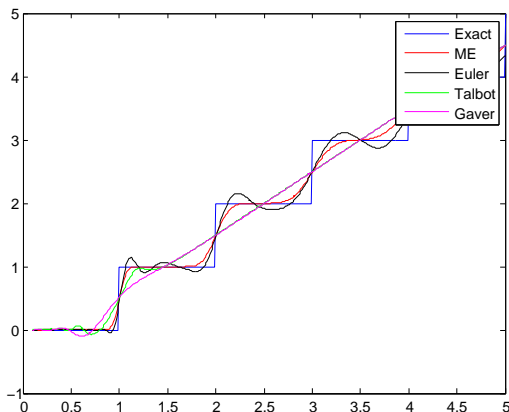
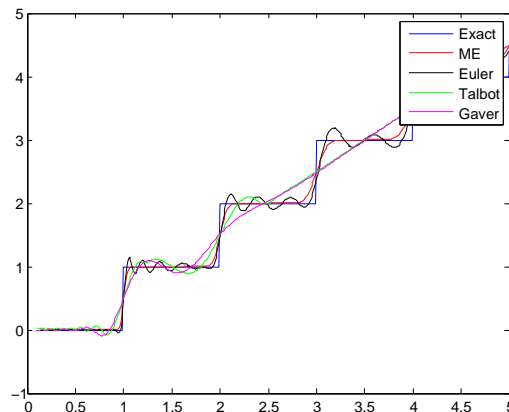


Figure 14. $h(t) = \mathbf{1}(t > 1)$ for $n = 24$ (Euler: $n = 25$)

Figures 15 and 16 depict the approximations for the shifted exponential function $\mathbf{1}(t > 1)e^{1-t}$ for order $n = 13$ ($n = 14$ for Gaver–Stehfest) and $n = 24$ ($n = 25$ for Euler) respectively. The Talbot method was omitted again. Similarly to Figures 13 and 14, the Gaver–Stehfest and the Euler methods overshoot again, and the matrix exponential method provides the best approximation overall.


 Figure 15. $h(t) = \mathbb{1}(t > 1)e^{1-t}$ for $n = 13$ (Gaver: $n = 14$)

 Figure 16. $h(t) = \mathbb{1}(t > 1)e^{1-t}$ for $n = 24$ (Euler: $n = 25$)

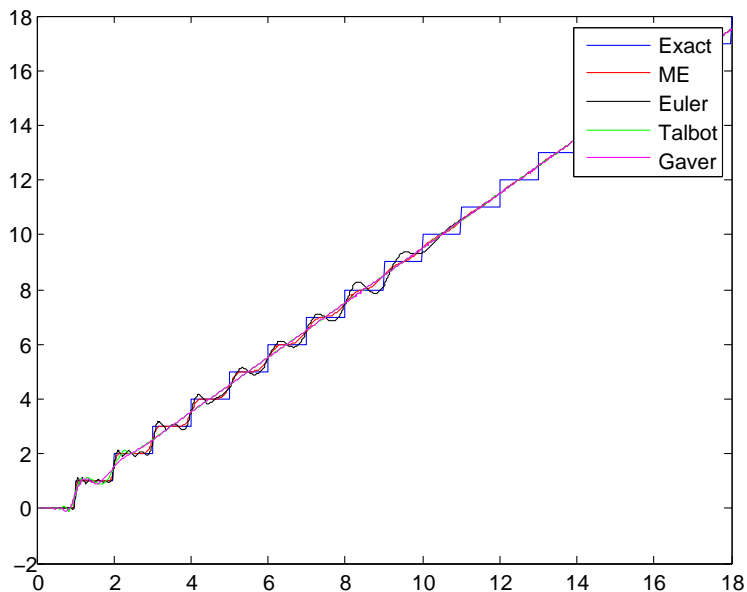
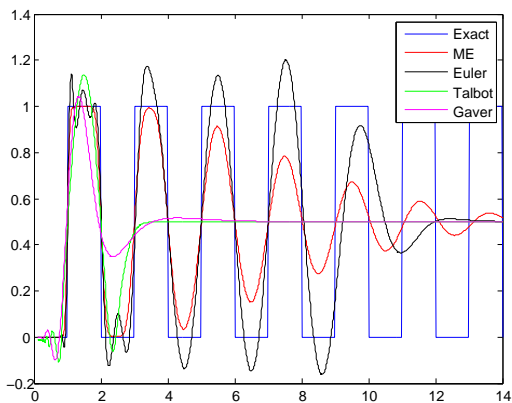
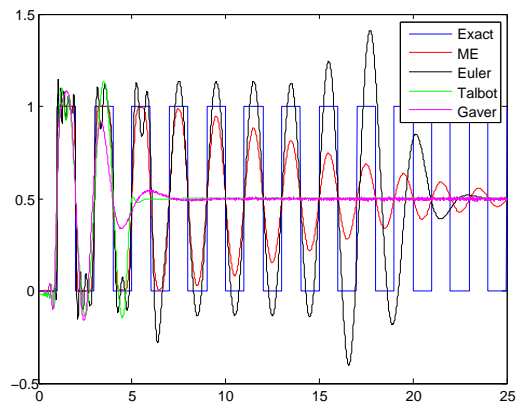
Figures 17 and 18 depict the approximations for the stepping function $h(t) = \lfloor t \rfloor$ for order $n = 13$ ($n = 14$ for Gaver–Stehfest) and $n = 24$ ($n = 25$ for Euler) respectively. Note that the error increases with t , and asymptotically, all approximating functions become linear (see Figure 19). The Gaver–Stehfest method provides a poor approximation by converging very fast to the linear asymptote; the other methods provide a reasonable approximation, but both the Euler and Talbot methods overshoot, and the Euler method has a considerable error even at the middle of the steps (halfway between jumps). The matrix exponential method provides a good approximation without overshooting.


 Figure 17. $h(t) = \lfloor t \rfloor$ for $n = 13$ (Gaver: $n = 14$)

 Figure 18. $h(t) = \lfloor t \rfloor$ for $n = 24$ (Euler: $n = 25$)

Figures 20 and 21 depict the approximations for the square wave function for order $n = 13$ ($n = 14$ for Gaver–Stehfest) and $n = 24$ ($n = 25$ for Euler and Talbot) respectively, with Figure 22 zooming in on smaller values of t . Similarly to $h(t) = \sin(t)$, the Talbot and Gaver methods provide a poor approximation, with both functions close to constant after very few periods. The Euler method provides relatively accurate approximation for 4 periods for $n = 14$ and 7 periods for $n = 25$. The overshooting of the Euler, Talbot and Gaver–Stehfest methods is evident again.

Similarly to $h(t) = \sin(t)$, the matrix exponential method retains the periodicity (along with the period length), does not overshoot, but the amplitude decays gradually.

In Table 3, the absolute maximal error for $h(t) = e^{-t}$ is compared for the various

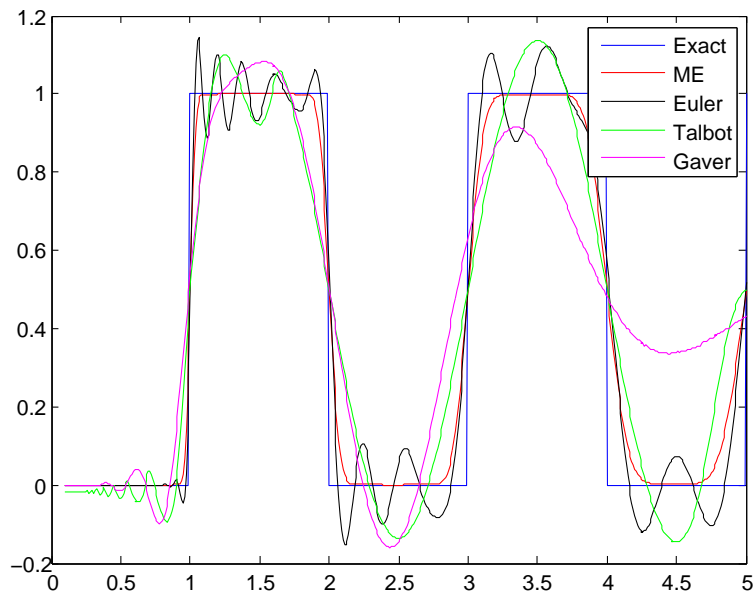

 Figure 19. $h(t) = [t]$ for $n = 24$ (Euler: $n = 25$)

 Figure 20. square wave function for $n = 13$ (Gaver: $n = 14$)

 Figure 21. square wave function for $n = 24$ (Euler, Talbot: $n = 25$)

methods for various orders. For this measure, the Talbot method outperforms the other, with the matrix exponential method and the Gaver–Stehfest method performing similarly and the Euler method worse than the others. (Note that the absolute maximal error makes sense only when $h(t)$ is continuous and has a linear asymptote, which is valid only for e^{-t} from among the test functions examined.)

h	n	ME	Euler	Talbot	Gaver
e^{-t}	3	0.0230	0.1841	0.0086	0.0334
	5	0.007423	0.03915	0.0003	0.006858

 Table 3
 Errors for $h(t) = e^{-t}$ in $\|\cdot\|_\infty$

In Table 4, the $\|\cdot\|_2$ errors in the interval $(0, 14)$ for each test function were examined. The table reflects the conclusion of the figures that the Euler method occasionally outperforms the matrix exponential method for periodic functions, but this error measure of the matrix exponential method is also close to the best one in each case.


 Figure 22. square wave function for $n = 24$ (Euler, Talbot: $n = 25$)

h	n	ME	Euler	Talbot	Gaver
e^{-t}	3	0.03909	0.08237	0.01206	0.03864
	5	0.01233	0.02139	0.0003876	0.01064
$\sin t$	13	3.248	3.345	4.548	4.597
	24	1.611	0.2538	4.168	4.405
$\mathbf{1}(t > 1)$	13	0.102	0.1012		0.1957
	24	0.06643	0.07439		0.1473
$\mathbf{1}(t > 1)e^{1-t}$	13	0.1022	0.1013		0.197
	24	0.06647	0.07442		0.1453
$[t]$	13	0.3984	0.356	0.5683	0.582
	24	0.2914	0.295	0.5131	0.5372
square wave function	13	1.24	1.273	1.702	1.719
	24	0.8226	0.7228	1.569	1.604

 Table 4
 Errors in $\|\cdot\|_2$ in the interval $(0, 14)$

6 Conclusion

Laplace transform functions are often used in stochastic and probability models, where a numerical inverse transformation method with overshooting might result in negative values or values larger than 1. In this work we propose a numerical inverse Laplace transformation method without overshooting based on recent results on matrix exponential distributions, which on one hand falls into the Abate–Whitt framework and inherits some of its main properties (e.g. light computational complexity) and on the other hand reduces the error of the previously applied non-overshooting alternative, the “Erlang” method (cf. (10) and (11)).

References

- [1] Joseph Abate, Gagan L. Choudhury, and Ward Whitt. *An Introduction to Numerical Transform Inversion and Its Application to Probability Models*, pages 257–323. Springer US, Boston, MA, 2000.

- [2] S. Asmussen and M. Bladt. Renewal theory and queueing algorithms for matrix-exponential distributions. In *Matrix-analytic methods in stochastic models*, volume 183 of *Lecture Notes in Pure and Appl. Math.*, pages 313–341, 1997.
- [3] Soren Asmussen, Florin Avram, and Miguel Usabel. Erlangian approximations for finite-horizon ruin probabilities. *ASTIN Bulletin*, 32(2):267281, 2002.
- [4] Aldous David and Shepp Larry. The least variable phase type distribution is erlang. *Stochastic Models*, 3(3):467–473, 1987.
- [5] D. P. Gaver. Observing stochastic processes and approximate transform inversion. *Oper. Res.*, 14:444459, 1966.
- [6] Illés Horváth, Orsolya Sáfár, Miklós Telek, and Bence Zámbo. *Concentrated Matrix Exponential Distributions*, pages 18–31. Springer International Publishing, Cham, 2016.
- [7] Illés Horváth, Orsolya Sáfár, Miklós Telek, and Bence Zámbo. List of coefficients for Matrix Exponential distributions with minimal coefficient of variation. <http://webspn.hit.bme.hu/~telek/techrep/mecoefficients.zip>, 2017. [Online; accessed 3-July-2017].
- [8] W. Whitt J. Abate. A unified framework for numerically inverting laplace transforms. *INFORMS Journal on Computing*, 18(4):408–421, Fall 2006.
- [9] V. Ramaswami, Douglas G. Woolford, and David A. Stanford. The erlangization method for markovian fluid flows. *Annals of Operations Research*, 160(1):215–225, Apr 2008.
- [10] H. Stehfest. Algorithm 368: Numerical inversion of laplace transforms [d5]. *Commun. ACM*, 13(1):47–49, January 1970.
- [11] A. Talbot. The accurate numerical inversion of laplace transforms. *IMA Journal of Applied Mathematics*, 23(1):97, 1979.
- [12] J. Abate Valko, P. P. Comparison of sequence accelerators for the gaver method of numerical laplace transform inversion. *Comput. Math. Appl.*, 48:629636, March 2004.
- [13] Quanrong Wang and Hongbin Zhan. On different numerical inverse laplace methods for solute transport problems. *Advances in Water Resources*, 75:80 – 92, 2015.